SCIENCE CHINA Materials ARTICLES

mater.scichina.com link.springer.com

Published online 4 November 2019 | https://doi.org/10.1007/s40843-019-1189-7

Sci China Mater 2020, 63(3): 383–391

Self-catalyzed growth of GaSb nanowires for high performance ultraviolet-visible-near infrared photodetectors

Kai Zhang[1,3], Ruiqing Chai[1,2], Ruilong Shi[1,2], Zheng Lou[1] and Guozhen Shen[1,2*]

ABSTRACT **A simple self-catalyzed chemical vapor deposition process was conducted to synthesize single-crystalline GaSb nanowires, where Ga droplets were utilized as the catalysts. The as-grown GaSb nanowires exhibited typical p-type semiconductor behavior with the calculated hole mobility of about 0.042 $cm^2 V^{-1} s^{-1}$. The photoresponse properties of the GaSb nanowires were studied by fabricating nanowire photodetectors on both rigid and flexible substrates. The results revealed that the photodetectors exhibited broad spectral response ranging from ultraviolet, visible, to near-infrared region. For the device on rigid substrate, the corresponding responsivity and the detectivity were calculated to be 3.86×10^3 A W^{-1} and 3.15×10^{13} Jones for 500 nm light, and 7.22×10^2 A W^{-1} and 5.90×10^{12} Jones for 808 nm light, respectively, which were the highest value compared with those of other reported $Ga_{1-x}In_xAs_ySb_{1-y}$ structure nanowires. Besides, the flexible photodetectors not only maintained the comparable good photoresponse properties as the rigid one, but also possessed excellent mechanical flexibility and stability. This study could facilitate the understanding on the fundamental characteristics of self-catalyzed grown GaSb nanowires and the design of functional nano-optoelectronic devices based on GaSb nanowires.**

Keywords: GaSb nanowires, chemical vapor deposition, mobility, photoresponse, near-infrared, flexible

INTRODUCTION

III–V semiconductor nanowires (NWs), such as InP, InAs, GaSb and InSb NWs, have attracted great research interests, due to their unique physical properties including narrow bandgap structures, specific crystal structures of the blende or wurtzite phase, high conductivity and large carrier motility [1–13]. They have been widely applied in high-speed field effect transistors (FETs), photodetectors, photovoltaics, light emitters and so on [2,12,14]. Especially, GaSb NW as an important p-type semiconductor, has narrow direct bandgap (~0.726 eV) and the highest hole mobility among all III-V group materials, recognized as the key basic units of nanoelectronics, such as high-speed FETs, infrared imaging devices, thermoelectric sensors, and infrared photodetectors [5,7,15–17].

GaSb NWs were usually synthesized by molecular beam epitaxy (MBE), metal-organic chemical vapor deposition (MOCVD), thermal decomposition or CVD methods with gold as the catalysts [4,9,18–20]. For instance, Yu *et al.* [18] grew GaSb NWs on Si substrates by MBE technique. Utilizing MOCVD technology, GaSb/GaAs core/shell NWs were synthesized on {111}B GaAs substrates by Guo *et al.* [19]. Yang *et al.* [4] synthesized single-crystalline GaSb NWs with a hole mobility of 200 $cm^2 V^{-1} s^{-1}$ *via* surfactant-assisted CVD process. These processes usually need gold as catalyst. As we know, gold is incompatible with the common complementary metal oxide semiconductor (COMS) technique, which greatly limits the application of GaSb NWs in large scale semiconductor device integration [21–23]. Thanks to the successful production of single-crystalline GaSb NWs, researchers could be able to investigate the electronic properties of the NWs and use them as high performance electronic devices. However, the photoresponse properties of GaSb NWs are usually not as good as other semiconductor NWs mainly due to the high dark current

[1] State Key Laboratory of Superlattices and Microstructures, Institution of Semiconductors, Chinese Academy of Sciences, Beijing 100083, China
[2] Center of Materials Science and Opto-electronic Engineering, University of Chinese Academy of Sciences, Beijing 100029, China
[3] Hebei Key Lab of Optic-electronic Information and Materials, the College of Physics Science and Technology, Hebei University, Baoding 071002, China
* Corresponding author (email: gzshen@semi.ac.cn)

induced by the natural high hole mobility of GaSb NWs, which hinders the high detectivity for the incident light [4,7,21,24,25]. Therefore, it is highly desirable to develop catalyst-free method to produce high-quality GaSb NWs with improved photoresponse properties.

In this work, a simple self-catalyzed CVD method was utilized to synthesize GaSb NWs with Ga droplets as the impurity-free catalysts. The as-grown GaSb NWs exhibit typical p-type semiconductor behaviour with a calculated hole mobility of about 0.042 $cm^2\ V^{-1}\ s^{-1}$. Besides, the GaSb NWs possess good photoresponse to lights with broad wavelengths ranging from ultraviolet, visible, to near-infrared region. The responsivity and the detectivity were calculated to be 3.86×10^3 A W^{-1} and 3.15×10^{13} Jones for 500 nm light, and 7.22×10^2 A W^{-1} and 5.90×10^{12} Jones for 808 nm light, respectively. The detectivity not only improves about four orders of magnitude compared with our previously reported gold-catalyzed GaSb NWs, but also is 1–2 orders of magnitude higher than that of other $Ga_{1-x}In_xAs_ySb_{1-y}$ NWs. To reveal the origin of the high photoresponse, the electric field distribution of the GaSb NWs was simulated using three-dimensional (3D) finite difference time domain (FDTD) methods. Flexible photodetectors were also fabricated, which not only maintained the analogous good photoresponse properties as the rigid one, but also exhibited excellent mechanical flexibility and stability.

EXPERIMENTAL SECTION

A horizontal quartz tube furnace was used to synthesize GaSb NWs, as illustrated in Fig. S1. Commercial GaSb powders were placed in the heating center of the furnace. (100) Si wafer coated with 8 nm Ga film was utilized as the substrate, which was put 20 cm away from the heating center in the downstream region. In order to remove the air of the quartz tube, the furnace was first pumpted to 1×10^{-2} torr, and then flowed with N_2/H_2 gas (volume ratio 9:1) with a constant flux of 50 sccm. The temperature of the furnace was increased to 800°C in 45 min and kept for 2 h. After being cooled down to room temperature (RT), NWs were found to deposit on the whole substrate, as shown in Fig. S2a. The morphology of the synthesized sample was characterized by a field-emission scanning electron microscope (SEM, Hitachi S4800). The microstructures and composition were investigated with a transmission electron microscope (TEM, JEOL JEM-3000F) equipped with energy dispersive spectroscopy (EDS).

GaSb NW-based photodetectors were fabricated on both rigid Si substrate coated with a layer of 300 nm SiO_2 and flexible polyimide (PI) substrate according to our previous reports [25–27]. The patterns of electrodes (Au 60 nm) were fabricated by the conventional photolithography, thermal evaporation, and lift-off process. The channel width was 10 μm, as shown in Fig. S3. The photoelectric signals were collected from the source and drain electrodes at a given bias during the incident light irradiation. As an FET device, the underlying Si substrate would act as the back gate. The device performance was measured on a Keithley 4200-SCS semiconductor test system connected to a probe station. The incident light source was a power adjustable homogeneous light source system (a xenon lamp 500W) and a monochromator (7ISW301). The Ophir NOVA power meter was employed to test the power density of the incident light. All the measurements were conducted in open atmosphere at RT (25°C).

RESULTS AND DISCUSSION

The mechanism of the self-catalyzed growth of GaSb NWs can be illustrated as shown in Fig. 1a and b. During the CVD process, Ga droplets were rapidly formed on the Si substrate due to its low melting point. When the GaSb source was heated to 800°C, GaSb vapor formed and was carried by the gas to the low temperature region and deposited on the Si substrate downstream. With the catalytic effects of Ga droplets, GaSb NWs then grew governed by the typical vapor-liquid-solid (VLS) mechanism [28]. To manifest the VLS process, the (100) Si wafer with 8 nm Ga film was annealed at 800°C under N_2/H_2 atmosphere. As shown in Fig. S2b, it is obvious that Ga droplets formed, which acted as the catalysts during the growth of GaSb NWs. Fig. 1c is the SEM image of the as-grown GaSb NWs. NWs with tapered structures deposit on the whole substrate, which are analogous to the previous report [20]. The lengths of the tapered GaSb NWs are 10–20 μm and the diameters are several hundred nanometers varied along the length of the NWs. Fig. 1d depicts the TEM image of a single GaSb NW. The tapered structure can be clearly seen, in good agreement with the SEM result. Droplet is attached to the top of the NW, confirming the VLS mechanism. EDS analysis was implemented on the rectangular zone shown in Fig. 1d inset. It is obvious that Ga and Sb elements are distributed uniformly on both "stick NW" and "top nanoparticle", which reveals the formation of GaSb NWs. Fig. 1e is the high-resolution TEM (HRTEM) image taken from Fig. 1d. The high distinct lattice fringes are presented and the spacing distances are 0.34, 0.29 and 0.20 nm, corresponding to the (111), (002), and (220) of GaSb with the

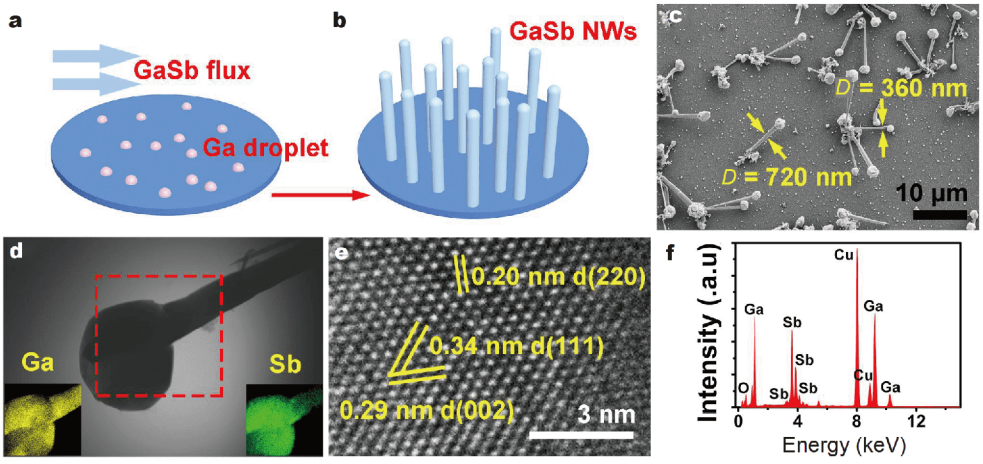

Figure 1 (a, b) Growth mechanism, (c) SEM, (d) TEM, (e) HRTEM image and (f) EDX spectrum of the self-catalyzed GaSb NWs.

zinc blende phase (PDF#07-0215). Fig. 1f depicts the EDS data of the rectangular zone in Fig. 1d. Except for very weak peaks of O and Cu from environment, all peaks are indexed to Ga and Sb, which further identifies the formation of GaSb NWs.

To investigate the electrical and photoresponse performances of the as-grown GaSb NWs, single NW FETs/photodetectors were fabricated on Si/SiO_2 substrate as described in the Experimental section. Fig. 2a demonstrates the structure of the device where the 300 nm SiO_2 is the dielectric layer and the monocrystalline Si (100) is the back gate. Different from common Ni, Ni/Au or Ti/Au electrodes [4,8,23], 60 nm Au was used as the electrode to build Schottky barrier between the electrodes and the GaSb NWs in order to decrease dark currents. Fig. 2b is the drain current (I_d) *versus* the source-drain voltage (V_d) curve under a dark condition. The back-to-back Schottky contacts could be observed obviously [29]. Fig. 2c displays the I_d and the gate current (I_g) *versus* the gate voltage (V_g) curves at a given V_d = 5 V. It is evident that the value of I_d is 1–2 orders of magnitude higher than that of I_g, exhibiting a well electrical property of the FET device. From the I_d-V_g curve, I_d is obviously decreased with the increased V_g, affirming the p-type semiconductor behavior of the as-synthesized GaSb NWs [4,8,23,30]. The threshold voltage (V_T) is at around 11.3 V. From the linear regime of the I_d-V_g curve, the transconductance (g_m) could be attained by the equation [25,31]:

$$g_m = dI_d / dV_g. \quad (1)$$

The transconductance was calculated as 0.3 nA V^{-1}. Therefore, the field-effect hole mobility μ_h of the GaSb NW-based FET could be acquired by the following equations [25,31,32]:

$$C_i \approx \frac{2\pi\varepsilon_0\varepsilon_r L}{\ln(2h/r)}, \quad (2)$$

$$\mu_h = \frac{g_m L^2}{V_d C_i}, \quad (3)$$

where C_i is the back gate capacitance, ε_0 is the vacuum dielectric constant (ε_o = 8.85×10^{-12} F m^{-1}), ε_r is the relative dielectric constant of SiO_2 (ε_r = 3.9), L is the GaSb NW length in the channel (10 μm), h is the thickness of SiO_2 dielectric layer (300 nm), and r is the radius of the NW (175 nm). The hole mobility μ_h could thus be calculated to be 0.042 cm^2 V^{-1} s^{-1}.

In Fig. 2d, the currents *versus* the voltage (*I*-*V*) curves of the GaSb NW-based photodetector were measured under monochromatic lights with the wavelengths ranging from 300 to 808 nm. Compared with the dark currents, all the photocurrents curves have been significantly elevated. The responsivity (R_λ) and the external quantum efficiency (EQE) are significant criteria for the detection properties of photodetectors, which can be defined by the following equations [14,25–27,33]:

$$R_\lambda = \frac{\Delta I}{P*S} = \frac{I_{photo} - I_{dark}}{P*S}, \quad (4)$$

$$EQE = R_\lambda * \frac{hc}{e\lambda}, \quad (5)$$

where P is the power intensity of incident light, S is the effective illumination area, I_{photo} and I_{dark} are the photocurrent and the dark current, h is Planck's constant, c is velocity of light, e is elementary electronic charge, λ is the wavelength of incident light. To eliminate the impacts of incident wavelength power intensities on the above *I*-*V*

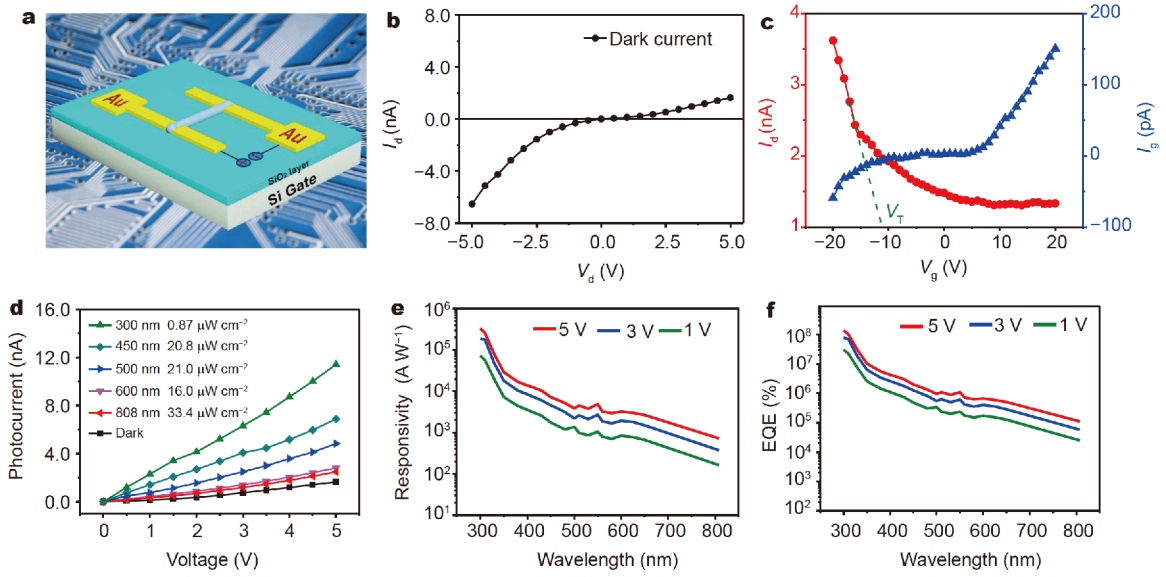

Figure 2 (a) Schematic illustration of the back-gate GaSb NW based FET device. (b) I_d-V_d curves of the FET under the dark condition. (c) I_d-V_g and I_g-V_g curves of the device at V_d = 5 V. (d) With V_g = 0 V, *I-V* curves of the GaSb NW-based photodetector under various incident lights from 300 to 808 nm, and dark conditions, respectively. (e, f) The spectral responsivity and EQE of the device at different biases of 5, 3 and 1 V, respectively.

curves, the power intensities were normalized by the R_λ equations in Fig. S4a. In Fig. 2e, f, the spectral photoresponse was measured at the bias of 5, 3 and 1 V, respectively. We can see that the GaSb NWs show obvious response to lights covering all the wavelengths from ultraviolet to near-infrared region, due to its narrow bandgap of 0.726 eV. Thus, the as-grown GaSb NWs may be good candidates for broad spectral response photodetectors. From Fig. S4a and Fig. 2e, f, the R_λ/EQE values decrease with increasing incident wavelength, which is in consistent with the GaSb NWs synthesized with Au catalysts and InAs NWs grown by MBE method [8,34]. At 5 V bias, the R_λ are 3.33×10^5 A W^{-1} for 300 nm, 3.86×10^3 A W^{-1} for 500 nm, and 7.22×10^2 A W^{-1} for 808 nm; the EQE are 1.38×10^8% for 300 nm, 9.58×10^5% for 500 nm and 1.11×10^5% for 808 nm, respectively.

Illuminated with visible and near-infrared light, the photoresponse performances of the GaSb NW-based photodetector were investigated systematically, as depicted in Fig. 3. Fig. 3b depicts the *I-V* curves of the device under 500 nm light with varied power intensities from 10.2 to 22.6 μW cm^{-2} as well as dark condition, respectively. The photocurrents were found to increase gradually with increasing light intensities. The relationship between photocurrent and light intensity is shown in Fig. 3c with a power law of $I_{PD} \sim P^{0.22}$, where I_{PD} is the photocurrent [25,27]. It means that the increase of the I_{PD} would be gradually slow down with the enhancement of the *P*. The dynamic photoresponse of the device to 500 nm light with varied light intensities of 10.2, 14.0 and 22.6 μW cm^{-2} are exhibited in Fig. 3d, respectively, where the photocurrents *versus* time (*I-t*) curves are recorded at 5 V bias by periodically turning the light on and off. Under the same power light, the photocurrents increase to the saturated state when the light shines, and then recover the original state when the light turns off periodically. Meanwhile, the saturated photocurrents are increased with the light power enhanced. Similarly, the *I-t* curves are also tested by turning on and off 500 nm light with 22.6 μW cm^{-2} at various biases of 5, 4 and 3 V in Fig. S4b. The photocurrents are also at "on" and "off" state regularly and increase with voltage elevated. The good reproducibility and stability of these *I-t* curves manifest good photoresponse of GaSb NWs to 500 nm light. Under the visible light of 600 nm with 16.0 μW cm^{-2}, the *I-t* curves which have good photoresponse were measured in Fig. 3e. Similarly, Fig. 3f shows the *I-t* curves have good photoresponse under near-infrared 808 nm light with 33.4 μW cm^{-2}. The response time was investigated with the enlarged one cycle *I-t* curves of 500 and 808 nm, respectively shown in Fig. S5. Defined as from 10% to 90% of photocurrents peak value, the reponse time for 500 and 808 nm light is 3.55 and 8.68 s, respectively. The relative slow response time in near-infrared region may result from the feeble incident power [2,17].

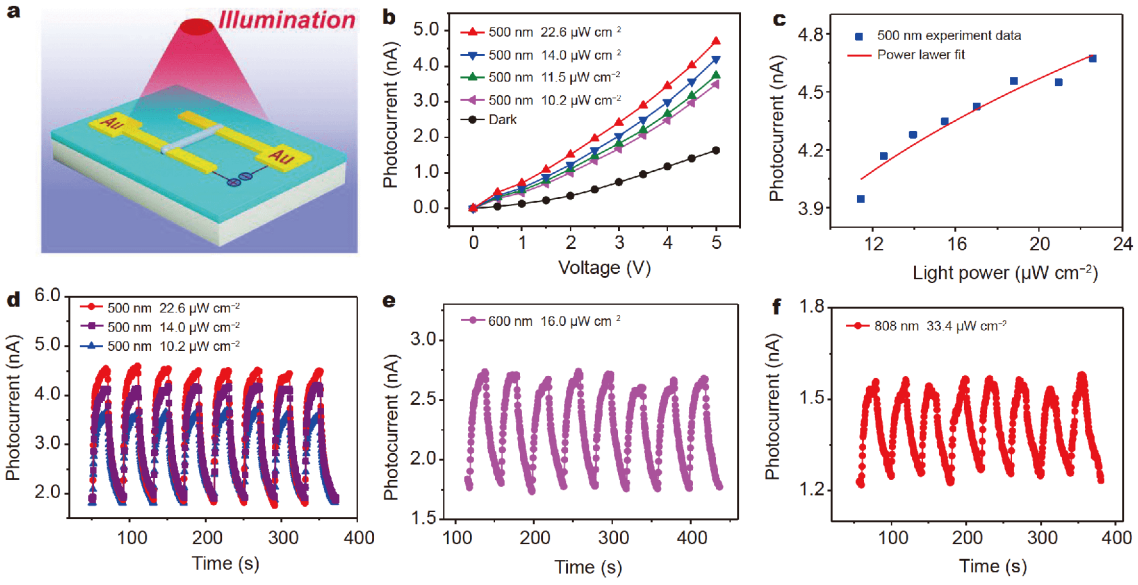

Figure 3 Photoresponse performances of the GaSb NW-based photodetector to visible and near-infrared lights, respectively. (a) Schematic illustration of the as-fabricated GaSb NW photodetector. (b) *I-V* curves of the device under 500 nm light with different power intensities; (c) *I-P* plot at 5 V bias, $I_{PD} \sim P^{0.216}$. (d) *I-t* curves of the device at 5 V bias under 500 nm light with the varied light intensities of 10.2, 14.0, and 22.6 μW cm^{-2}, respectively. (e) *I-t* curves at 5 V bias under 600 nm light. (f) *I-t* curves at 5 V bias under 808 nm light.

The detectivity (D^*) is the vital parameter for photodetectors, which is defined as follows [24–27, 33]:

$$D^* = R_\lambda \left(\frac{S\Delta f}{2eI_{dark}} \right)^{1/2}, \quad (6)$$

where Δf is the band width. From the data acquired from Figs 2 and 3, the I_{light}/I_{dark}, R_λ, EQE, and D^* of the GaSb NW based photodetectors to lights with different wavelengths are summarized in Table 1, further confirming the excellent photoresponse properties for broad spectrum of the as-synthesized GaSb NWs.

Table 2 compares the photoresponse performances of the current self-catalyzed GaSb NWs with those of several typically reported III-V NWs, including GaSb NWs, InAs NWs, InP NWs, and other ternary III-V NWs. From the Table, we can see that the present GaSb NWs exhibit obvious enhanced properties. With higher R_λ and EQE, our GaSb NWs have noticeable improved value of D^*, which is about 1–2 orders of magnitude higher than that of InAs NWs, GaSb NWs, and ternary $Ga_{1-x}In_xAs_ySb_{1-y}$ NWs. Besides, all the values of R_λ, EQE and D^* increase drastically compared with our previously reported Au-catalyzed GaSb NWs [8]. The photoresponse enhancement results from two reasons. One is the self-catalyzed grown GaSb NWs without other elements impurity. The other reason is that the separate Au electrode is adopted to build Schottky barrier which decreases the dark currents.

Table 1 Summary of the I_{light}/I_{dark}, R_λ, EQE and D^* of the GaSb NW-based photodetector

Wavelength (nm)	I_{light}/I_{dark}	R_λ (A W^{-1})	EQE (%)	D^* (Jones)
300	7.0	3.33×105	1.38×108	2.72×1015
450	4.2	7.21×103	1.99×106	5.89×1013
500	3.0	3.86×103	9.58×105	3.15×1013
600	2.1	3.25×103	6.71×105	2.65×1013
650	1.7	2.67×103	5.09×105	2.18×1013
808	1.5	7.22×102	1.11×105	5.90×1012

Due to the lightweight, portable, and foldable properties, flexible electronic devices have intrigued the enthusiasm of scholars in the last decade [41]. To study the possible application of the present GaSb NWs for flexible electronics, photodetectors were then fabricated on flexible PI substrate as shown in Fig. 4a. Fig. 4b shows the *I-V* curves of the flexible photodetector under dark condition as well as under various lights with wavelengths ranging from 300 to 808 nm. The flexible device has obvious response to lights with wide wavelengths including ultraviolet, visible and near-infrared lights. Similar to the device on silicon substrate, the photoresponse performances of the flexible one also decrease with increased incident wavelength as shown in Fig. S6a. The photocurrents of flexible device are rather lower than that of the

Table 2 Structure, growth method, and photoresponse performance of several typical III-V NWs-based detectors

Matrial	Growth method	Detectivity wavelength (nm)	Operating temperature	Dark current	R_λ (A W^{-1})	EQE (%)	D^* (Jones)	Ref.
GaSb	CVD	300–800	RT	-	443.3	688.4	2.86×10^{9}	8
InAs	CVD	300–1100	RT	-	4.4×10^{3}	1.03×10^{6}	2.6×10^{11}	14
InAs	MBE	830–3133	77–460 K	~30 pA@0.2 V bias	~60	-	$\sim10^{12}$	2
InP	CVD	500–1200	RT	8 pA@1 V	2.8×10^{5}	4.2×10^{7}	9.1×10^{15}	35
InGaAs	CVD	1100–2000	RT	144 nA@0.5 V	6.5×10^{3}	5.04×10^{5}	-	36
GaAsSb	CVD	1160–1550	RT	~200 nA@1 V	1.7×10^{3}	1.62×10^{5}	-	37
InGaSb	CVD	500–1550	RT	1.9 μA@2 V	6.0×10^{3}	4.8×10^{6}	3.7×10^{9}	38
GaInAsSb	CVD	980	RT	~200 nA@1 V	675	8.05×10^{4}	-	39
GaInAsSb	CVD	980	RT	~150 nA@1 V	158	2.0×10^{4}	-	40
GaSb/GaInSb core-shell	CVD	1100–2200	RT	10 nA@−1 V	1.05×10^{3}	8.5×10^{6}	-	17
GaSb	CVD	300–808	RT	1.6 nA@5 V	3.86×10^{3}	9.58×10^{5}	3.15×10^{13}	This work

rigid device due to the worse contact between Au electrodes and the flexible PI substrate according to previous reports [25–27]. Fig. 4c shows the *I-t* curves of the flexible device under 500 nm light irradiation with the power intensities of 10.2, 14.0 and 22.6 μW cm^{-2}, respectively. The *I-t* curve of the device under 300 nm incident light with the intensity of 0.87 μW cm^{-2} was also carried out and shown in Fig. S6b. All the curves exhibit good reproducibility and stability, indicating the excellent stability of the flexible device. The photocurrents increase with the elevated light power and the relationship can be fitted by the power law $I_{PD} \sim P^{0.26}$, as depicted in Fig. 4d, analogous to that of the rigid device. The EQE of the flexible device is 1.72×10^{5}% and 2.96×10^{4}% for 500 and

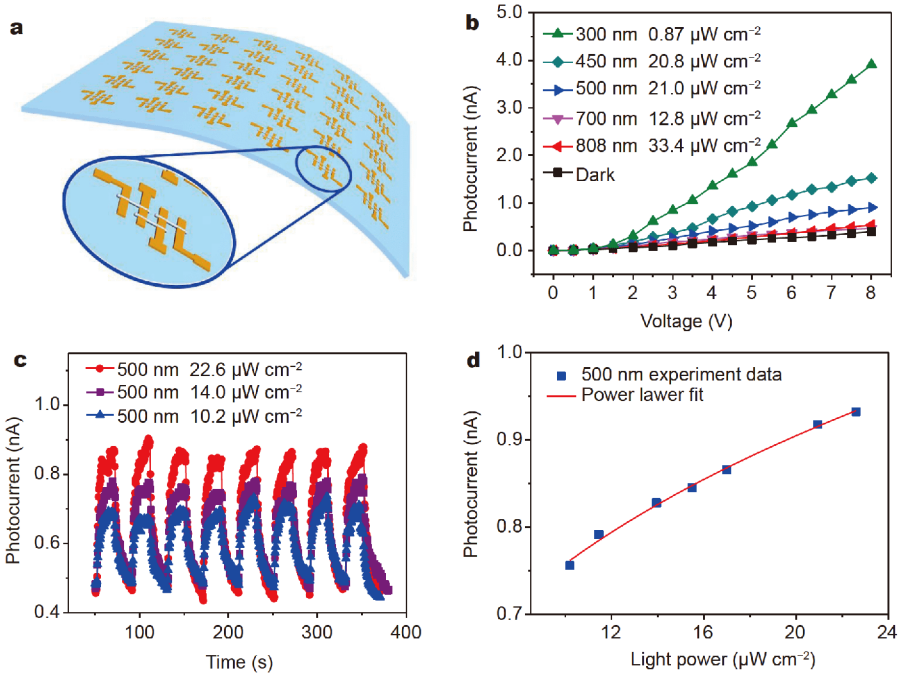

Figure 4 Photoresponse properties of GaSb NWs-based flexible photodetectors to visible and near-infrared light illuminations. (a) The schematic of the GaSb NWs-based photodetectors on flexible PI substrate. (b) *I-V* curves of the flexible photodetectors illuminated with incident light from 300 to 808 nm, and under the dark condition. (c) *I-t* curves of the flexible photodetectors at 8 V bias under 500 nm light with 10.2, 14.0, 22.6 μW cm^{-2}; (d) *I-P* plot at 8 V bias, $I_{PD} \sim P^{0.26}$.

808 nm light, respectively. The D^* is 1.14×10^{13} and 4.90×10^{12} Jones for the 500 and 808 nm light, respectively. These parameters are comparable to those of the rigid device on silicon substrate, confirming the good photoresponse properties of the GaSb NW-based flexible photodetectors.

The mechanical and electrical stabilities are very important parameters for real applications of flexible devices. By setting the flexible photodetectors on a movable stage, we can bend the device at different angles, as shown in Fig. S7. By the simulation of MATLAB software, the bending angle is thus defined, as depicted in Fig. 5a. The θ_1 and θ_2 are the angles between the tangent and the horizontal direction, thus the bending angle θ is the sum of θ_1 and θ_2. Fig. 5b is the stability data of saturated photocurrents when the flexible device is irradiated with 500 and 800 nm light under various bending angles, respectively. The saturated photocurrents under different bending angles are quite stable, indicating the good electrical stabilities of the flexible device. Fig. 5c and d are the *I-V* curves of the flexible device with the bending angles of 0°, 30°, 60°, 90° and 120°, when irradiated with 500 and 808 nm lights, respectively. All of the curves fit well with each other, confirming the excellent mechanical flexibility and electrical stabilities of the GaSb-NW based flexible device.

To investigate the photoelectric conversion properties of the GaSb NWs in detail, the electric field distribution of the NW was simulated using 3D FDTD when the NW was illuminated with 808 nm light. Fig. 6a and b are the $|E_z|$ distribution in *X-Y* and *Y-Z* planes. In Fig. 6a, it is easy to find that the electric field intensity is weakened along the direction of the incident light. The active area is mainly near the surface of the GaSb NW, consistent with the classical theory of 1D photodetection [14,24,26]. The photon-generated electron-hole pairs result in desorption of oxygen molecules which are adsorbed on the surfaces of the NW. Therefore, the space electric field distribution near the NW surface is changed [24,26,42]. Meanwhile, the photocurrent will be boosted due to the remaining free carriers in the NW. Fig. 6b is the *Y-Z* plane where the *X* position is −80 nm. Although the electric field intensity is relatively feeble, the dominant surface behavior could be clearly observed. The great mass of incident photons could be absorbed to generate electron-hole pairs, resulting in the photoelectric conversion near the surface of the NW.

CONCLUSIONS

In summary, GaSb NWs were grown successfully in a conventional CVD system *via* a self-catalyzed approach. The as-synthesized GaSb NWs possessed a typical p-type semiconductor character with the hole mobility of 0.042 $cm^2\ V^{-1}\ s^{-1}$ and wide spectral response from ul-

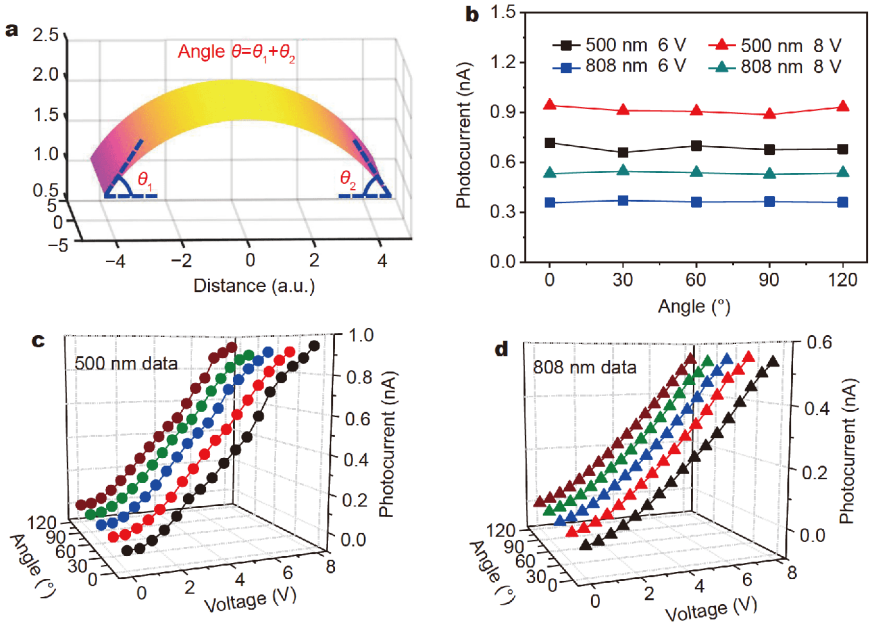

Figure 5 (a) Diagram of the flexible photodetector bending simulated *via* MATLAB software and the defined bending angle θ. (b) Stability of the saturated photocurrents under various bending angles. (c, d) *I-V* curves of the flexible photodetetetor under 500 and 808 nm light irradiation by bending it with 0°, 30°, 60°, 90° and 120°, respectively.

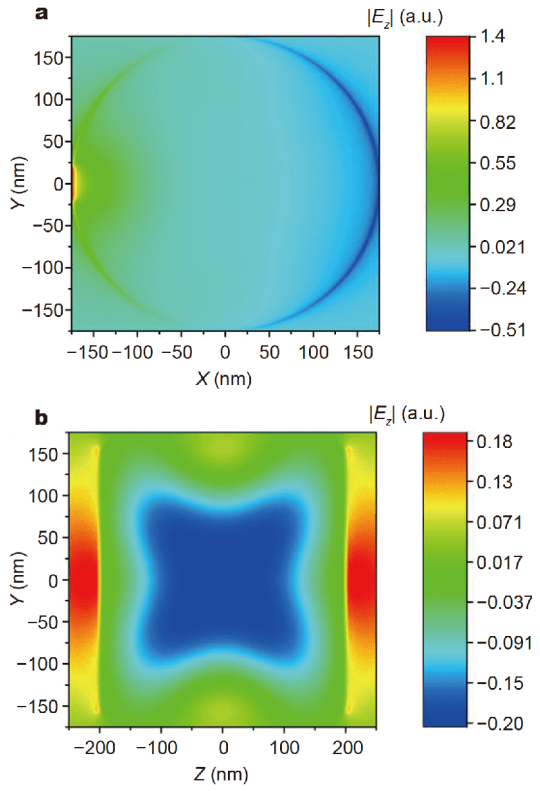

Figure 6 Under the incident near-infrared 808 nm light, the electric field distribution of the GaSb NWs simulated *via* FDTD method. (a) The electric intensity in the *X*-*Y* plane, and (b) the electric intensity in the *Y*-*Z* plane with $X = -80$ nm.

traviolet to near-infrared region. Both rigid and flexible photodetectors were fabricated on the GaSb NWs. And studies found that, for the 500 nm visible light and 808 nm near-infrared light, the rigid device exhibited large responsivity of 3.86×10^3 A W^{-1} and 7.22×10^2 A W^{-1}, high external quantum efficiency of 9.58×10^5% and 1.11×10^5%, ultrahigh detectivity of 3.15×10^{13} and 5.90×10^{12} Jones, respectively. The flexible photodetectors also demonstrated good photoresponse properties as well as excellent mechanical and electrical flexibilities. To elucidate the origin of the superb photoresponse performances, a simulation of the electric field distribution of the GaSb NW under 808 nm light was implemented *via* the FDTD method, and the result was in consistence with the classical 1D photodetection theory.

Received 1 August 2019; accepted 20 September 2019; published online 4 November 2019

1 Novotny CJ, Yu ET, Yu PKL. InP nanowire/polymer hybrid photodiode. Nano Lett, 2008, 8: 775–779
2 Fang H, Hu W, Wang P, *et al.* Visible light-assisted high-performance mid-infrared photodetectors based on single InAs nanowire. Nano Lett, 2016, 16: 6416–6424
3 Guo N, Hu W, Liao L, *et al.* Anomalous and highly efficient InAs nanowire phototransistors based on majority carrier transport at room temperature. Adv Mater, 2014, 26: 8203–8209
4 Yang ZX, Han N, Fang M, *et al.* Surfactant-assisted chemical vapour deposition of high-performance small-diameter GaSb nanowires. Nat Commun, 2014, 5: 5249
5 Yang Z, Liu L, Yip SP, *et al.* Complementary metal oxide semiconductor-compatible, high-mobility, 111-oriented GaSb nanowires enabled by vapor–solid–solid chemical vapor deposition. ACS Nano, 2017, 11: 4237–4246
6 Ek M, Borg BM, Johansson J, *et al.* Diameter limitation in growth of III-Sb-containing nanowire heterostructures. ACS Nano, 2013, 7: 3668–3675
7 Yang Z, Yip SP, Li D, *et al.* Approaching the hole mobility limit of GaSb nanowires. ACS Nano, 2015, 9: 9268–9275
8 Luo T, Liang B, Liu Z, *et al.* Single-GaSb-nanowire-based room temperature photodetectors with broad spectral response. Sci Bull, 2015, 60: 101–108
9 Burke RA, Weng X, Kuo MW, *et al.* Growth and characterization of unintentionally doped GaSb nanowires. J Elec Mater, 2010, 39: 355–364
10 Pan D, Fan DX, Kang N, *et al.* Free-standing two-dimensional single-crystalline InSb nanosheets. Nano Lett, 2016, 16: 834–841
11 Mattias Borg B, Wernersson LE. Synthesis and properties of antimonide nanowires. Nanotechnology, 2013, 24: 202001
12 Zhang Y, Wu J, Aagesen M, *et al.* III–V nanowires and nanowire optoelectronic devices. J Phys D-Appl Phys, 2015, 48: 463001
13 Vurgaftman I, Meyer JR, Ram-Mohan LR. Band parameters for III–V compound semiconductors and their alloys. J Appl Phys, 2001, 89: 5815–5875
14 Liu Z, Luo T, Liang B, *et al.* High-detectivity InAs nanowire photodetectors with spectral response from ultraviolet to near-infrared. Nano Res, 2013, 6: 775–783
15 Plis EA, Kutty MN, Myers S, *et al.* Performance improvement of long-wave infrared InAs/GaSb strained-layer superlattice detectors through sulfur-based passivation. Infrared Phys Tech, 2012, 55: 216–219
16 Kim C, Kurosaki K, Muta H, *et al.* Thermoelectric properties of Zn-doped GaSb. J Appl Phys, 2012, 111: 043704
17 Ma L, Hu W, Zhang Q, *et al.* Room-temperature near-infrared photodetectors based on single heterojunction nanowires. Nano Lett, 2014, 14: 694–698
18 Yu X, Li L, Wang H, *et al.* Two-step fabrication of self-catalyzed Ga-based semiconductor nanowires on Si by molecular-beam epitaxy. Nanoscale, 2016, 8: 10615–10621
19 Guo YN, Zou J, Paladugu M, *et al.* Structural characteristics of GaSb/GaAs nanowire heterostructures grown by metal-organic chemical vapor deposition. Appl Phys Lett, 2006, 89: 231917
20 Schulz S, Schwartz M, Kuczkowski A, *et al.* Self-catalyzed growth of GaSb nanowires at low reaction temperatures. J Cryst Growth, 2010, 312: 1475–1480
21 Zamani RR, Gorji Ghalamestani S, Niu J, *et al.* Polarity and growth directions in Sn-seeded GaSb nanowires. Nanoscale, 2017, 9: 3159–3168
22 Jeppsson M, Dick KA, Nilsson HA, *et al.* Characterization of GaSb nanowires grown by MOVPE. J Cryst Growth, 2008, 310: 5119–5122
23 Ganjipour B, Nilsson HA, Mattias Borg B, *et al.* GaSb nanowire

single-hole transistor. Appl Phys Lett, 2011, 99: 262104
24 Soci C, Zhang A, Xiang B, *et al.* ZnO nanowire UV photodetectors with high internal gain. Nano Lett, 2007, 7: 1003–1009
25 Chen G, Liang B, Liu X, *et al.* High-performance hybrid phenyl-C61-butyric acid methyl ester/Cd_3P_2 nanowire ultraviolet–visible–near infrared photodetectors. ACS Nano, 2014, 8: 787–796
26 Zhang K, Luo T, Chen H, *et al.* Au-nanoparticles-decorated Sb_2S_3 nanowire-based flexible ultraviolet/visible photodetectors. J Mater Chem C, 2017, 5: 3330–3335
27 Lou Z, Li L, Shen G. Ultraviolet/visible photodetectors with ultrafast, high photosensitivity based on 1D ZnS/CdS heterostructures. Nanoscale, 2016, 8: 5219–5225
28 Shen G, Chen PC, Bando Y, *et al.* Pearl-like ZnS-decorated InP nanowire heterostructures and their electric behaviors. Chem Mater, 2008, 20: 6779–6783
29 Wang X, Zhang Y, Chen X, *et al.* Ultrafast, superhigh gain visible-blind UV detector and optical logic gates based on nonpolar *a*-axial GaN nanowire. Nanoscale, 2014, 6: 12009–12017
30 Dutta PS, Bhat HL, Kumar V. The physics and technology of gallium antimonide: An emerging optoelectronic material. J Appl Phys, 1997, 81: 5821–5870
31 Cui Y, Duan X, Hu J, *et al.* Doping and electrical transport in silicon nanowires. J Phys Chem B, 2000, 104: 5213–5216
32 Yu G, Liang B, Huang H, *et al.* Contact printing of horizontally-aligned p-type Zn_3P_2 nanowire arrays for rigid and flexible photodetectors. Nanotechnology, 2013, 24: 095703
33 Gong X, Tong M, Xia Y, *et al.* High-detectivity polymer photodetectors with spectral response from 300 nm to 1450 nm. Science, 2009, 325: 1665–1667
34 Miao J, Hu W, Guo N, *et al.* Single InAs nanowire room-temperature near-infrared photodetectors. ACS Nano, 2014, 8: 3628–3635
35 Zheng D, Wang J, Hu W, *et al.* When nanowires meet ultrahigh ferroelectric field–high-performance full-depleted nanowire photodetectors. Nano Lett, 2016, 16: 2548–2555
36 Tan H, Fan C, Ma L, *et al.* Single-crystalline InGaAs nanowires for room-temperature high-performance near-infrared photodetectors. Nano-Micro Lett, 2016, 8: 29–35
37 Ma L, Zhang X, Li H, *et al.* Bandgap-engineered GaAsSb alloy nanowires for near-infrared photodetection at 1.31 μm. Semicond Sci Technol, 2015, 30: 105033
38 Li D, Lan C, Manikandan A, *et al.* Ultra-fast photodetectors based on high-mobility indium gallium antimonide nanowires. Nat Commun, 2019, 10: 1664
39 Chen X, Li H, Qi Z, *et al.* Synthesis and optoelectronic properties of quaternary GaInAsSb alloy nanosheets. Nanotechnology, 2016, 27: 505602
40 Li MZ, Chen XL, Li HL, *et al.* Optoelectronic properties of single-crystalline GaInAsSb quaternary alloy nanowires. Chin Phys B, 2018, 27: 078101
41 Liu Z, Xu J, Chen D, *et al.* Flexible electronics based on inorganic nanowires. Chem Soc Rev, 2015, 44: 161–192
42 Li L, Lou Z, Shen G. Hierarchical CdS nanowires based rigid and flexible photodetectors with ultrahigh sensitivity. ACS Appl Mater Interfaces, 2015, 7: 23507–23514

Acknowledgements This work was supported by the National Natural Science Foundation of China (61574132 and 61625404).

Author contributions Zhang K and Shen G designed the devices and experiments; Zhang K performed the experiments; Zhang K, Chai R, Shi R, and Lou Z analyzed the data; Zhang K wrote the paper with support from Shen G. All authors contributed to the general discussion.

Conflict of interest The authors declare no conflict of interest.

Supplementary information Supporting data are available in the online version of the paper.

Kai Zhang received his PhD degree from the Institute of Semiconductors, Chinese Academy of Sciences in 2018. He joined Hebei University as an assistant professor in 2018. His current research focuses on low dimensional semiconductor electronics, including transistors, photodetectors, photovoltaic and lasers.

Guozhen Shen received his BSc degree in 1999 from Anhui Normal University and PhD degree in 2003 from the University of Science and Technology of China. From 2004 to 2013, he conducted his research in Hanyang University (Korea), National Institute for Materials Science (Japan), University of Southern California (USA) and Huazhong University of Science and technology (China). He joined the Institute of Semiconductors, Chinese Academy of Sciences as a professor in 2013. His current research focuses on flexible electronics and printable electronics, including transistors, photodetectors, sensors and flexible energy-storage devices.

自催化生长GaSb纳米线及其在高性能紫外-可见-近红外光电探测器中的应用

张凯[1,3], 柴瑞青[1,2], 史瑞龙[1,2], 娄正[1], 沈国震[1,2*]

摘要 本文应用镓金属液滴作为催化剂, 采用化学气相沉积方法自催化合成了单晶GaSb纳米线. 研究表明该GaSb纳米线为典型的p型半导体, 霍尔迁移率为> 0.042 $cm^2\ V^{-1}\ s^{-1}$. 硅基和柔性衬底上构筑的基于GaSb纳米线的光电探测器, 具有良好的紫外-可见-近红外宽光谱探测性能. 硅基器件对500 nm的可见光响应率可达3.86×10^3 A W^{-1}, 探测率可达3.15×10^{13} Jones; 柔性器件在保持相似光电性能的同时, 具有极好的机械柔韧性和稳定性. 本文有助于更好地揭示自催化生长的GaSb纳米线的性能, 并为进一步设计基于GaSb纳米线的功能光电器件打下了实验基础.

